ACS OMEGA

http://pubs.acs.org/journal/acsodf

Article

Absorption and Spreading of a Liquid Droplet Over a Thick Porous Substrate

Rachid Chebbi*

Cite This: *ACS Omega* 2021, 6, 4649−4655

Read Online

ACCESS | Metrics & More | Article Recommendations

ABSTRACT: Spreading over porous substrates occurs in several processes including printing, cleaning, coating, and manufacturing of ceramic structures. For small drops, viscous and capillary forces are ultimately the predominant forces. The process typically undergoes three phases: a first stage in which the droplet spreads, a second phase in which the area of contact with the solid substrate nearly remains constant, and a third stage in which the droplet retracts with its volume reaching zero finally. The objective of the investigation is to find the dynamics of spreading and absorption of the droplet using fundamentals while making relevant approximations to account for both radial and vertical dynamics. The proposed model requires minimal computational work. The results are compared with the published experimental data for the perfect wetting case, and are found to be in good agreement with detailed published experimental data for both droplet dynamics and dynamics of penetration in the porous substrate.

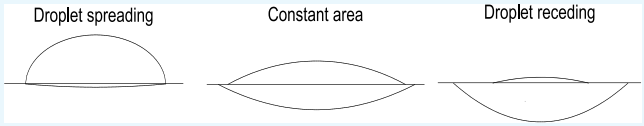

1. INTRODUCTION

The dynamics of spreading and penetration is important in a number of cases including ink-jet and 3D-printing, clean-up processes, coating of porous substrates, irrigation, and manufacture of ceramic structures.[1−3] In ink-jet printing, spreading produces blurring and in clean-up processes penetration should be limited.[1] The dynamics of spreading over an impermeable wall are reviewed in Rosenholm[4] and the references therein. For the case of perfect wetting, the works of Chebbi and Selim[5] and Chebbi,[6] extending those of Starov et al.[7] and Hervet and de Gennes[8] that include disjoining pressure effects, provide very good agreement with experimental data.

This research is concerned with the dynamics of spreading and imbibition of a porous substrate. Reviews of spreading and penetration into porous media can be found in Gambaryan-Roisman,[3] Rosenholm,[4] Alleborn and Raszillier,[9] and Daniel and Berg,[10] with a focus on spreading and penetration into paper in the article by Rosenholm.[4] In the case of ink-jet printing, splashing occurs if Weber's number is larger than 50, which is not typically the case.[11] A review of previous works involving droplet impact on a porous substrate can be found in Choi et al.[12]

Starov et al.[13] showed experimentally the existence of two to three stages, as spreading and penetration into the porous medium are competing processes. In the first stage (IDA), the contact area between the liquid droplet and the porous substrate (drawing area) increases. The first stage is followed by a second stage in which the drawing area remains constant (CDA), and finally by a third stage in which the contact line recedes resulting in a decrease in the drawing area (DDA). The wet part of the porous substrate is modeled as a spherical cap, and the experimental data include the radii of the contact and wetted areas along with the contact angles of the droplet and the imbibed part. The results presented in a dimensionless form show very close profiles for different viscosities of the silicon oil used with the same glass filter material, and for different materials (metal and glass filters) having nearly the same porosity and average pore size for using the same silicon oil viscosity. Differences in the dimensionless curves for the radii of the droplet contact area and the wetted circle at the interface between air and the wetted part of the porous substrate are presented.

Based on the scope of the present work addressing wetting of porous media by a perfectly wetting liquid, the emphasis is on spreading and imbibition of thick and initially dry porous substrates. Different models have been used. They differ in the scope of the work, assumptions used, and simplifications included to allow for more analytical treatment. The dynamics has two competing processes: spreading and penetration. As far as spreading is concerned, the lubrication approximation requiring a small contact angle is used in Davis and Hocking,[1] and Alleborn and Raszillier.[9] The actual contact angle is assumed constant in Davis and Hocking,[1] and the apparent contact angle is assumed to be given by the molecular-kinetic theory in Clarke et al.[11] and a modified Hoffman−Voinov−Tanner law in Hilpert and Ben-David.[14] To model the flow near

Received: November 2, 2020
Accepted: January 26, 2021
Published: February 5, 2021

the contact line, the precursor film and disjoining pressure concepts are used in Alleborn and Raszillier,[9] and the no-slip boundary condition is adopted in Davis and Hocking.[1] As far as the dynamics of penetration is concerned, the flow is modeled as occurring in vertical capillary tubes. The Washburn (also called Lucas−Washburn) equation is used in Holman et al.[2] and Denesuk et al.,[15] and Darcy's law is utilized in Alleborn and Raszillier[9] and Clarke et al.[11] Denesuk et al.[15] considered two cases, CDA and DDA, and Holman included the IDA case. The solutions for the contact area radius and the droplet contact angle in Clarke et al.[11] were found to depend on a friction parameter, with the advancing contact angle ranging between 38.9 and 51.9°, and a third parameter depending on the porous substrate. The three parameters were determined to get the best fit with the experimental data obtained. The power law of a linear function of time for the contact area radius was found by curve fitting against experimental data in Holman et al.[2] The work of Hilpert and Ben-David[14] for the wetting case (excluding perfect wetting) requires fitting against the experimental data in a modified Hoffman−Voinov−Tanner law. Inclusion of both vertical and axial liquid motion requires computational fluid dynamics, and the solution was obtained using a finite element method in Alleborn and Raszillier.[9] A finite-difference numerical model was used by Navaz et al.[16] to find the capillary pressure considering a two-phase flow without the restriction of having a sharp front between the penetrating liquid and the air. Lattice Boltzmann numerical solutions were used by Frank and Perré.[17]

Oko et al.[18] used high-speed digital imaging and showed that in a dimensionless form, inkjet penetrating volume in controlled glass membranes varies with time to the power of 0.8 at intermediate times. Tan[19] performed experimental and numerical investigations and concluded the existence of three stages including spreading, wicking, and evaporation occurring at the microsecond, millisecond, and second time scales, respectively, for picoliter droplets. Liu et al.[20] noticed that imbibition in a compressed bed predominantly occurs at the constant contact area and provided a universal dimensionless relation for the imbibed liquid volume versus time. Barui et al.[21] investigated the dynamics of ethylene glycol−water solution penetration in alumina powder bed using X-ray imaging. Washburn-based models were found consistent with experimental data using a semi-empirically determined porosity correction factor.[21]

The present work provides a model addressing the complexity of a penetrating liquid from a droplet over a thick porous medium using an analytical approach and relevant approximations, while requiring very limited computational work and providing results that are consistent with experimental data. The complexity of the problem arises from the flow dynamics over the porous medium, coupled with penetration in a complex network of capillaries leading to penetration in both axial and radial directions. The governing equations are presented first, followed by a presentation and discussion of the results for the case of a perfectly wetting liquid case.[13,22] The model results are validated against extensive data[13,22] and conclusions are provided. To the author's knowledge, such an extensive validation and comparison has not been addressed in the literature so far.

2. COMPUTATIONAL METHODS

The dynamics is subdivided into three phases. First, spreading occurs along with penetration of the liquid into the porous substrate. In the second phase, the droplet radius nearly remains constant. In the last phase, the droplet retracts. There is a continuous loss of mass by continuing penetration during the three phases till the mass of the droplet reaches zero.

2.1. Penetration in a Capillary Tube. Flow in small capillaries involves both inertia forces and viscous forces initially, with viscous forces remaining as the ultimate dominating resisting force in the remaining process. The Lucas−Washburn equation (also called Washburn equation)[23,24] assumes a constant contact angle, which is strictly valid at small contact line velocities.[11] The equation provides the penetration depth x into one straight capillary tube as

$$x = \sqrt{\frac{a\sigma \cos \alpha_s}{2\mu} t} \tag{1}$$

where a is the inner radius of the capillary tube and α_s is the static contact angle. A treatment involving the effect of the dynamic contact angle on the dynamics of penetration shows excellent agreement with the published experimental data.[25] The use of the concept of disjoining pressure shows excellent agreement with the experimental data for the relation between capillary number and dynamic contact angle in the case of perfect wetting case.[26]

2.2. Porous Medium Permeability. The porous substrate is characterized by its permeability defined by Darcy's equation for the superficial liquid velocity v_s (volumetric flow rate per unit area of porous medium) as a function of the pressure gradient dp/dx

$$v_s = -\frac{k}{\mu}\frac{dp}{dx} \tag{2}$$

In the case of penetration, the pressure gradient is obtained from the Young−Laplace equation as

$$-\frac{dp}{dx} = \frac{2\sigma \cos \alpha / a}{x} \tag{3}$$

To account for the porosity ϕ of the bed, we have

$$\phi\frac{dx}{dt} = \frac{k}{\mu}\frac{2\sigma \cos \alpha / a}{x} \tag{4}$$

Integrating eq 4 and comparing the expression for $x(t)$ with eq 1 provides the following expression for k

$$k = \frac{a^2}{8}\phi \tag{5}$$

The result is in agreement with ref 9.

Using the above expression for k along with the static contact angle approximation, the liquid depth takes the following form, consistent with ref 3

$$x = \zeta\sqrt{t} \quad \zeta = \sqrt{4\frac{k\sigma \cos \alpha_s}{\mu a \phi}} \tag{6}$$

2.3. Relations between Apex, Radius, and Volume. In the present work, the liquid droplet and the volume of the porous medium imbibed by the liquid are both assumed spherical in shape. The following relation applies to the spherical cap volumes of apex h_a and radius L[27]

$$h_a^3 + 3L^2h_a = \frac{6}{\pi}V \tag{7}$$

The following relations including the radius of curvature R_c and the contact angle θ can be easily derived

https://dx.doi.org/10.1021/acsomega.0c05341
ACS Omega 2021, 6, 4649−4655

$$2R_c = h_a + \frac{L^2}{h_a} \tag{8}$$

$$\cos\theta = 1 - \frac{h_a}{R_c} \tag{9}$$

In the case of thin droplets, the spherical cap can be approximated as a paraboloid. The angle and apex expressions can be simplified and eqs 7−9 reduce to

$$L^2 h_a = \frac{2}{\pi} V \tag{10}$$

$$2R_c = \frac{L^2}{h_a} \tag{11}$$

$$\frac{\theta^2}{2} = \frac{h_a}{R_c} \tag{12}$$

In the present treatment, the general equations 7−9 are used for the droplet. The approximations 10 and 11 can be used for the imbibed part of the porous medium since the contact angles considered are not large.

2.4. Combined Capillary Spreading with Penetration into a Permeable Substrate. A schematic figure of a drop spreading on a thick porous medium is given in Figure 1.

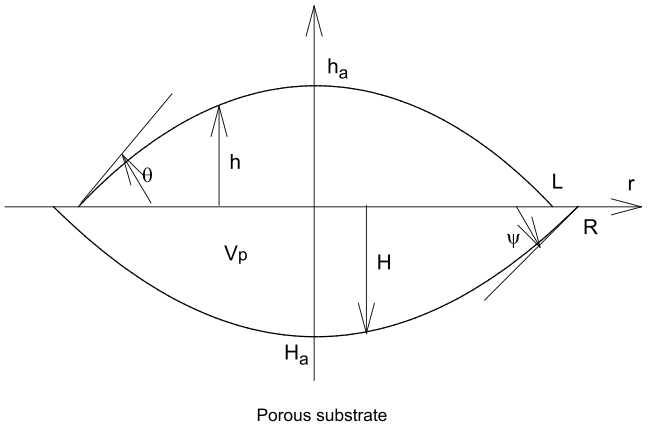

Figure 1. Schematic of a spreading drop on a porous substrate.

The fraction of the porous medium filled with liquid is denoted by ε_f. Using eqs 5 and 6, the effective k_e and ζ_e values are estimated as

$$k_e = k\frac{\varepsilon_f}{\phi}; \quad \zeta_e = C_f\zeta\sqrt{\frac{\varepsilon_f}{\phi}} \tag{13}$$

where C_f is a correction factor. The effective ζ_e is used instead of ζ in the following treatment.

Assuming one-dimensional penetration as an approximation, the rate of change in the volume of porous medium imbibed by the liquid is given by

$$\frac{dV_{pl}}{dt} = \varepsilon_f \frac{d}{dt}\left[\int_0^R H(2\pi r)dr\right] \tag{14}$$

where H is the depth of penetration at t and r.

Using the Leibniz formula yields

$$\frac{dV_{pl}}{dt} = \varepsilon_f \int_0^R \frac{\partial H}{\partial t}(2\pi r)dr + \varepsilon_f \frac{dR}{dt}H(t, R)\,(2\pi R) \tag{15}$$

The last term in eq 15 is zero, as the depth of penetration H is zero at L.

As in Clarke et al.,[11] we assume penetration to start at $\tau(r)$ defined as the time at which the leading edge reaches the radial distance r. Using eq 6 along with the unidirectional penetration approximation yields

$$\frac{\partial H}{\partial t} = \frac{\zeta_e}{2\sqrt{t - \tau(r)}} \tag{16}$$

Then, substituting into eq 15 while discarding the last term gives

$$\frac{dV_{pl}}{dt} = \varepsilon_f \int_0^L \zeta_e \frac{1}{2\sqrt{t - \tau(r)}}(2\pi r)dr \tag{17}$$

2.4.1. IDA Phase. Spreading over a permeable solid is approximated by the following expression

$$L = L_0 + \frac{\ln(t/t_0)}{\ln(t_{CDA}/t_0)}(L_{CDA} - L_0) \tag{18}$$

or piecewise by a linear function of $\ln(t)$ as needed. Using a mass balance, the remaining droplet volume, V, is obtained from the total liquid volume V_l and the liquid volume imbibed by the porous substrate, V_{pl}, as

$$V = V_l - V_{pl} \tag{19}$$

The values of V_{pl} can be obtained numerically through a series of time steps t_n (n starting at 1) using the discretized form of eq 17

$$V_{pl,n} = V_{pl,n-1} + \Delta t \times \varepsilon_f \zeta_e \sum_{i=1}^{n} \frac{\pi(L_i^2 - L_{i-1}^2)}{2\sqrt{t_n - \frac{t_i + t_{i-1}}{2}}} \tag{20}$$

Discretizing eqs 18 and 19 provides the radius of the droplet at t_n

$$L_n = L_0 + \frac{\ln(t_n/t_0)}{\ln(t_{CDA}/t_0)}(L_{CDA} - L_0) \tag{21}$$

and the updated value V_n

$$V_n = V_l - V_{pl,n} \tag{22}$$

Using eqs 7−9 yields the following expressions for the apex h_a and the contact angle θ

$$h_a = \sqrt[3]{\frac{3V}{\pi} + \sqrt{\frac{9V^2}{\pi^2} + L^6}} + \sqrt[3]{\frac{3V}{\pi} - \sqrt{\frac{9V^2}{\pi^2} + L^6}};$$
$$\theta = \arccos\left(\frac{L^2 - h_a^2}{L^2 + h_a^2}\right) \tag{23}$$

Making use of eq 23 along with the updated values L_n and V_n provides the updated values of h_a and the contact angle θ.

For small contact angles, the following simpler equations can be used

$$h_a = \frac{2V}{\pi L^2}; \quad \theta = \frac{4V}{\pi L^3} \tag{24}$$

The imbibed part of the porous medium, V_p, is partially filled with air, while the rest, V_{pl}, is filled with liquid. The volume, V_p, is obtained as $V_p = V_{pl}/\varepsilon_f$, where ε_f is calculated as

https://dx.doi.org/10.1021/acsomega.0c05341
ACS Omega 2021, 6, 4649−4655

$$\varepsilon_f = \frac{V_l}{\pi R_{max,e}^3 \psi_{max,e}/4} \tag{25}$$

using the final data for the wetted area radius at the interface between the porous medium and the air and the contact angle of the imbibed part of the liquid.

Using Darcy's law in the horizontal direction yields

$$\phi \frac{dR}{dt} = \frac{k_e}{\mu} \frac{p_c}{R - L} \tag{26}$$

where the capillary pressure p_c for zero contact angle is given by

$$p_c = \sigma \frac{2}{a} \tag{27}$$

Substituting for the capillary pressure p_c and using the definition of ζ_e yields R by a simple explicit integration of

$$\frac{dR}{dt} = \frac{\zeta_e^2}{2(R - L)} \text{ for } \psi \le \psi_{max} \tag{28a}$$

where ψ_{max} is max (ψ_V), with $\psi_V = 4V_p/(\pi R^3)$, or simple calculation using

$$R = \left(\frac{4V_p}{\pi \psi_{max}}\right)^{1/3} \text{ for } \psi = \psi_{max} \tag{28b}$$

The new radius of the imbibed part R is obtained by a simple explicit integration of eq 27.

The apex H_a of the imbibed part is obtained by integration of

$$\frac{dH_a}{dt} = \frac{\zeta_e}{2\sqrt{t}} \tag{29}$$

Substituting into eq 30 gives the updated value of the contact angle ψ

$$\psi = \max(2H_a/R, \psi_{max}) \tag{30}$$

The IDA phase starts at t_0 and ends at $t_{c,i}$. The spreading dynamics during this phase is obtained from a fit to experimental data. The contact angle of the droplet and the dynamics of penetration, including the contact angle and radius, are modeled.

2.4.2. CDA Phase. In case an intermediate constant drawing area phase is included in the analysis, L is approximately constant. Assuming that τ_{av} is small compared to t, and integrating eq 37 (derived in Section 2.4.3) yields

$$V = V_{CDA} - 2\pi L^2 \varepsilon_f \zeta_e (\sqrt{t} - \sqrt{t_{CDA}}) \text{ (approximate)} \tag{31}$$

For a recommended and more accurate integration, the following discretization equation can be used along with eq 21 to obtain $V_{pl,n}$.

$$V_{pl,n} = V_{pl,n-1} + \Delta t \times \varepsilon_f \zeta_e \sum_{i=1}^{N} \frac{\pi (L_i^2 - L_{i-1}^2)}{2\sqrt{t_n - \frac{t_i + t_{i-1}}{2}}} \tag{32}$$

L does not change during the second phase. Therefore, the summation does not include the terms $N + 1 - n$ since the corresponding terms are equal to zero.

The values of h_a and θ can be calculated using eqs 23 or 24 for a small contact angle. Using the approximate expression 31, we have for small θ

$$\theta = 4 \frac{V_{CDA} - 2\pi L^2 \varepsilon_f \zeta_e (\sqrt{t} - \sqrt{t_{CDA}})}{\pi L_{CDA}^3} \text{ (approximate)} \tag{33}$$

Integrating eq 28a yields for L constant (second phase)

$$R = L + \sqrt{L^2 + R_{CDA}^2 - 2LR_{CDA} + \zeta_e^2 (t - t_{CDA})} \tag{34}$$

To get more accurate results, eq 32 is recommended instead of eq 34, and used in the Results and Discussion Section. Using the volume of the imbibed part V_p (obtained from V) and R, H_a and ψ are obtained from eqs 29 and 30.

The time interval for the CDA phase is $t_{CDA} - t_{DDA}$. In the present model, the value of t_{DDA}, the time at which the CDA phase ends, is postulated to be the time at which ψ_H reaches ψ_{max} as discussed in Section 2.4.1. The value, θ_m, as defined in refs 13, 22, is determined at t_{CDA}.

2.4.3. DDA Phase. The droplet starts receding at a constant angle, θ_{DDA}, during the last phase.[13,22] In the present model, θ_{DDA}, is determined at $(t_{CDA} + t_{DDA})/2$ and used to determine $L(t)$ in the last phase as shown later. The average time considered corresponds to the case where the drop dynamics is considered as consisting of two stages only[13,22] (rather than three stages), in which the drop initially spreads, reaches a maximum value for L at $(t_{c,i} + t_{c,f})/2$, and then starts retracting at a constant angle. We can write eq 17 in the following form

$$\frac{dV_{pl}}{dt} = \varepsilon_f \pi L^2 \zeta_e \frac{1}{2\sqrt{t - \tau_{av}(t)}} \tag{35}$$

where the average τ_{av} is given by

$$\frac{1}{\sqrt{t - \tau_{av}(t)}} = \varepsilon_f \int_0^L \zeta_e \frac{1}{\sqrt{t - \tau(r)}} (2\pi r) dr \tag{36}$$

In the third phase, t is large compared to τ_{av}. Using this approximation, differentiating the mass balance eq 19 and combining it with eq 35 yields

$$\frac{dV}{dt} = -\varepsilon_f \pi L^2 \zeta_e \frac{1}{2\sqrt{t}} \tag{37}$$

Substituting for V as a function of the constant contact angle θ_{DDA} and L yields

$$\frac{dL}{dt} = -\frac{2\varepsilon_f \zeta_e}{3\theta_{DDA}} \frac{dt}{\sqrt{t - \tau_{av}(t)}} \tag{38}$$

Neglecting τ_{av} and integrating the above equation provides

$$L = L_{DDA} - \frac{4\varepsilon_f \zeta_e}{3\theta_{DDA}} (\sqrt{t} - \sqrt{t_{DDA}}) \tag{39}$$

As in Denesuk et al.,[15] L varies as a linear function of $\sqrt{t}$ in the DDA phase. The droplet radius and the apex h_a are given by

$$V = \frac{\pi \theta_{DDA} L^3}{4} \tag{40}$$

$$h_a = \theta_{DDA} \frac{L}{2} \tag{41}$$

The radius of the wetted area at the solid substrate surface R is determined using eqs 28a and 28b. The volume of the porous medium V_p is obtained as V_{pl}/ε_f. Using eqs 29 and 30, we can determine the apex H_a and ψ. The final time is reached when L is zero. Using eq 39 provides

https://dx.doi.org/10.1021/acsomega.0c05341
ACS Omega 2021, 6, 4649−4655

Table 1. Data and Calculated Values of Permeability k, ζ, and ζ_e[a]

run	material	porosity, ϕ	average pore size (μm)	viscosity, μ (P)	V_l (μL)	k (m^2)	ζ (m/s$^{1/2}$)	ζ_e (m/s$^{1/2}$)
2	glass	0.53	4.7	1	5.9	1.083×10^{-12}	0.590×10^{-3}	0.495×10^{-3}
3	glass	0.53	4.7	5	8.2	1.083×10^{-12}	0.264×10^{-3}	0.220×10^{-3}

[a]The data for the material, porosity, average pore size, viscosity, and liquid volume represent the work of Starov et al.[13] Adapted with permission from [Elsevier]. Copyright [2003] [Elsevier].

$$t_{max} = \left[\frac{3\theta_{DDA}}{4\varepsilon_f\zeta_e}L_{DDA} + \sqrt{t_{DDA}}\right]^2 \quad (42)$$

3. RESULTS AND DISCUSSION

The model results are compared with the experimental data for the case of perfect wetting of silicone oil droplets on thick porous glass filters in Starov et al.[13,22] The physical properties and characteristics of the porous medium are presented in Table 1.

The correction factor C_f for the cases referred to in Table 1 (ref 13) is taken as 0.707 ($=1/\sqrt{2}$), assuming the average pore size in ref 13 represents the average pore diameter, which is typically the case, and C_f is taken as 1 if the average pore size in ref 13 represents the average pore radius, which is less common. In both cases, ζ_e has the same value, and the results obtained and presented below are the same. The values of permeability k in Table 1 were obtained using the data in Starov et al.[13] for air flowing at a flux of 1.9 L/(min cm^2) and a pressure of 0.1 bar across a glass filter of 1.9 mm thick. The fraction of the porous medium filled with the liquid within the imbibed volume, ε_f, was calculated using eq 25 along with the experimental end values of ψ_{max} (39 grad for Run 2 and 42 grad for Run 3) and R_{max} (3.20 mm for Run 2 and 3.50 mm for Run 3). The values of ε_f were found to be 0.374 and 0.369 for Runs 2 and 3, respectively. The values of ζ and ζ_e were calculated using eqs 6 and 13 and are shown in Table 1. To calculate ζ, a surface tension value of 0.02 N/m was estimated.[7]

The experimental data for $L(t)$ during the IDA phase are approximated using the following expressions

$$\text{Run 2:} \quad L\ (\text{mm}) = 1.23 + \frac{\log(t/0.04)}{\log(1/0.04)}(2.27 - 1.23),$$

$$\text{for} \quad 0.04\ \text{s} \le t(\text{s}) \le 1\ \text{s}$$

Run 3:

$$L\ (\text{mm}) = 1.29 + \frac{\log(t/0.04)}{\log(0.35/0.04)}(1.60 - 1.29) \quad \text{for}$$

$$0.04\ \text{s} \le t(\text{s}) \le 0.35\ \text{s}$$

$$L\ (\text{mm}) = 1.60 + \frac{\log(t/0.35)}{\log(5/0.35)}(2.57 - 1.60),$$

$$\text{for } 0.35\ \text{s} \le t(\text{s}) \le 5\ \text{s}$$

Integration was performed using a time step Δt of 0.001 s for Run 2 and 0.01 s for Run 3. The initial conditions were obtained using the initial data at $t_0 = 0.04$ s for R and ψ. The value of R at t_0 was taken as 1.002 L to avoid singularity while using eq 28a. The values of ψ_{max} are found to be 0.613 rad (39.0 grad) for Run 2 and 0.614 rad (39.1 grad) for Run 3, compared to the experimental data: 39 grad and 42 grad for Runs 2 and 3, respectively (Figure 2).

The results for $L(t)$ and $R(t)$ for Runs 2 and 3 are shown in Figures 3 and 4, respectively.

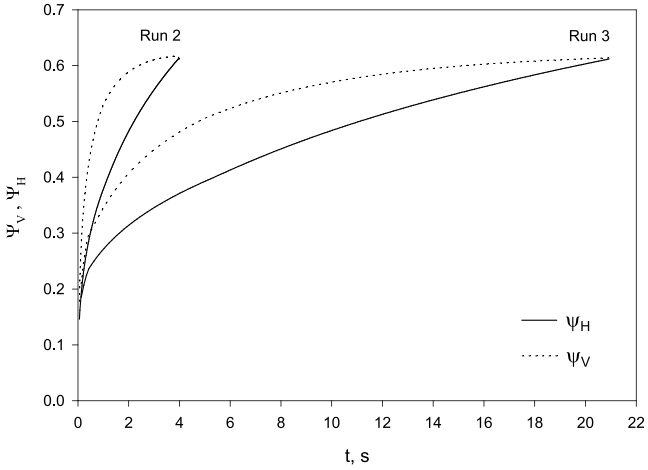

Figure 2. Results for ψ_H and ψ_V using the data for Runs 2 and 3 in Starov et al.[13] Adapted with permission from [Elsevier]. Copyright [2003] [Elsevier].

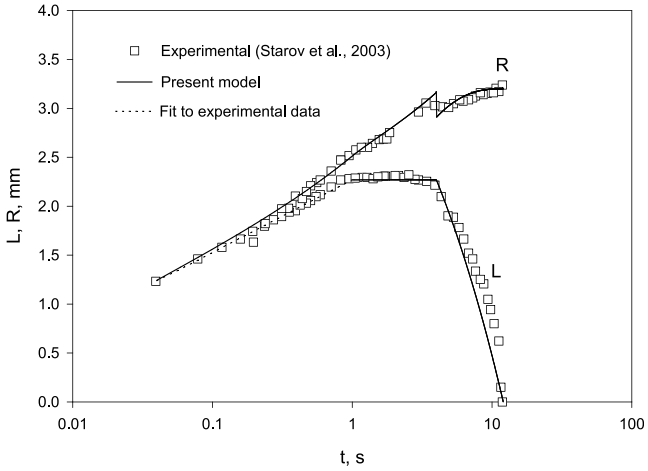

Figure 3. Results for L and R. Comparison with the experimental data for Run 2. The symbols represent the work of Starov et al.[13] Adapted with permission from [Elsevier]. Copyright [2003] [Elsevier].

The dotted lines represent the approximate profiles for $L(t)$ using the above expressions. The results (continuous lines) are found to be in good agreement with the experimental data. The profiles for L are approximated as flat (CDA phase) over the range 1−4 s for Run 2 and 5−20.9 s for Run 3 (Figures 3 and 4).

The sharp change occurring in the profile for R is due to the use of eq 28b instead of eq 28a when ψ_H reaches ψ_V (Figure 2), at which time ψ is considered as constant at larger times according to the present model. The change in the trend for the experimental values of R is more visible in Figure 3.

Figure 5 shows the variation of the droplet contact angle with time. The final values for θ_{DDA} are found to be 0.160 rad (10.2 grad) and 0.181 rad (11.5 grad) for Runs 2 and 3, respectively.

The results for ψ/ψ_{max} are plotted versus t/t_{max} in Figure 6.

https://dx.doi.org/10.1021/acsomega.0c05341
ACS Omega 2021, 6, 4649−4655

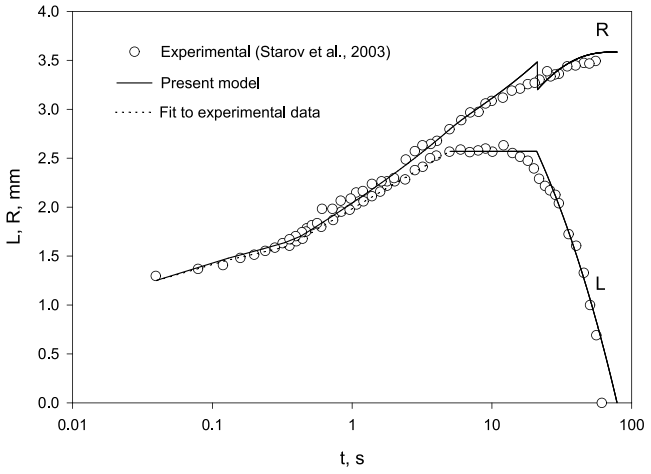

Figure 4. Results for L and R. Comparison with the experimental data for Run 3. The symbols represent the work of Starov et al.[13] Adapted with permission from [Elsevier]. Copyright [2003] [Elsevier].

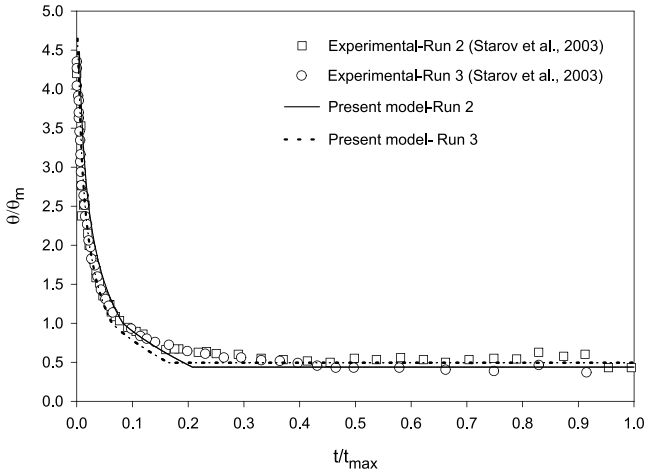

Figure 5. Results for θ as a function of time. Comparison with the experimental data for Runs 2 and 3. The symbols represent the work of Starov et al.[13] Adapted with permission from [Elsevier]. Copyright [2003] [Elsevier].

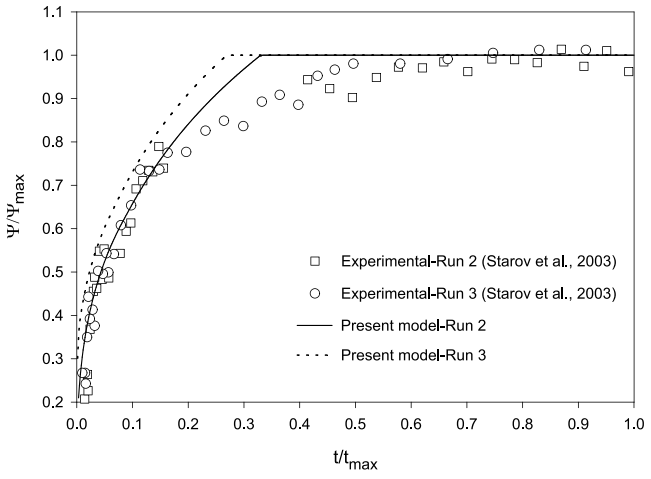

Figure 6. Results for ψ as a function of time. Comparison with the experimental data for Runs 2 and 3. The symbols represent the work of Starov et al.[13] Adapted with permission from [Elsevier]. Copyright [2003] [Elsevier].

Figures 3−6 show that the present results are in good agreement with the experimental data in refs 13, 23. In the case of low viscosity (Run 1,[13] viscosity = 0.05 P), the second stage is fast and is more difficult to observe experimentally.

The droplet profiles and the profiles for the porous medium part V_l containing the imbibed liquid V_{pl} in the pores (Figure 7) are obtained using

$$h = \sqrt{\frac{L^2}{\sin^2\theta} - r^2} - L\frac{|\cos\theta|}{\sin\theta} \tag{43}$$

$$H = \psi\frac{R}{2}\left(1 - \frac{r^2}{R^2}\right) \tag{44}$$

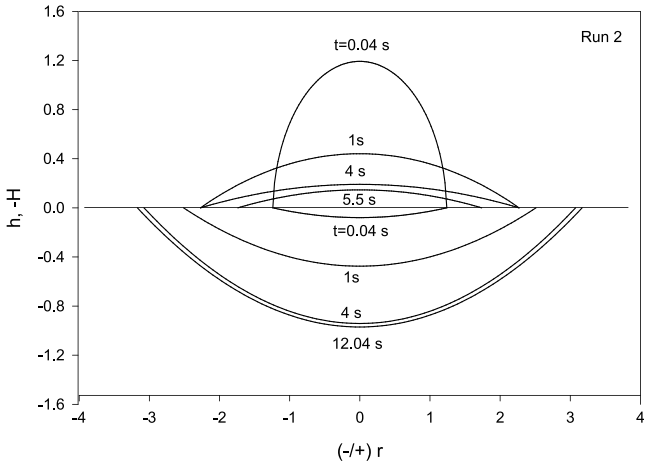

Figure 7. Profiles for the liquid drop, $h(r, t)$, and the wetted part of the porous substrate, $H(r, t)$, at different times for Run 2. The profiles at t = 0.04, 1, 4, 5.5, and 12.04 s, were determined starting from the initial time reported for Run 2 in Starov et al.[13] Adapted with permission from [Elsevier]. Copyright [2003] [Elsevier].

4. CONCLUSIONS

The three phases occurring during the absorption of a liquid over a thick porous medium (increasing, constant, and decreasing drawing area phases) are considered using an analytical model. The present model was developed assuming no or small changes in the properties including surface tension. The present model applies to the case of perfect wetting, small size drops (so that gravity effects can be dropped), and no/low volatility cases. In addition, the model does not include the very first stage of the process as inertia terms are neglected. Both axial and radial dynamics are included in the analysis. The results are found in good agreement with the extensive experimental data for both the drop dynamics and liquid penetration in the perfect wetting case of silicone oil droplets on thick porous glass filters.[13,22] The results include the droplet dynamics during the CDA and DDA phases and the dynamics of penetration during the IDA, CDA, and DDA phases. Investigation of the dynamics of spreading of the droplet over thick porous substrates during the first phase (IDA) is recommended in the future.

AUTHOR INFORMATION

Corresponding Author

Rachid Chebbi − *Department of Chemical Engineering, American University of Sharjah, Sharjah 26666, United Arab*

https://dx.doi.org/10.1021/acsomega.0c05341
ACS Omega 2021, 6, 4649−4655

Emirates; orcid.org/0000-0003-3673-3612; Phone: 971 6 515 2983; Email: rchebbi@aus.edu; Fax: 971 6 515 2979

Complete contact information is available at: https://pubs.acs.org/10.1021/acsomega.0c05341

Notes

The author declares no competing financial interest.

■ ACKNOWLEDGMENTS

This work was accomplished by the author at the American University of Sharjah. No research grant was requested or provided to complete the present work.

■ REFERENCES

(1) Davis, S. H.; Hocking, L. M. Spreading and Imbibition of Viscous Liquid on a Porous Base. II. *Phys. Fluids* **2000**, *12*, 1646−1655.
(2) Holman, R. K.; Cima, M. J.; Uhland, S. A.; Sachs, E. Spreading and Infiltration of Inkjet-Printed Polymer Solution Droplets on a Porous Substrate. *J. Colloid Interface Sci.* **2002**, *249*, 432−440.
(3) Gambaryan-Roisman, T. Liquids on Porous Layers: Wetting, Imbibition and Transport Processes. *Curr. Opin. Colloid Interface Sci.* **2014**, *19*, 320−335.
(4) Rosenholm, J. B. Liquid Spreading on Solid Surfaces and Penetration into Porous Matrices: Coated and Uncoated Papers. *Adv. Colloid Interface Sci.* **2015**, *220*, 8−53.
(5) Chebbi, R.; Selim, M. S. Capillary Spreading of Liquid Drops on Solid Surfaces. *J. Colloid Interface Sci.* **1997**, *195*, 66−76.
(6) Chebbi, R. Dynamics of Wetting. *J. Colloid Interface Sci.* **2000**, *229*, 155−164.
(7) Starov, V. M.; Kalinin, V. V.; Chen, J. D. Spreading of Liquid Drops over Dry Surfaces. *Adv. Colloid Interface Sci.* **1994**, *50*, 187−221.
(8) Hervet, H.; de Gennes, P. G. Dynamique du Mouillage: Films Précurseurs sur Solid 'Sec' (The Dynamics of Wetting: Precursor Films in the Wetting of Dry Solids). *C.R. Acad. Sci. II.* **1984**, *299*, 499−503.
(9) Alleborn, N.; Raszillier, H. Spreading and Sorption of a Droplet on a Porous Substrate. *Chem. Eng. Sci.* **2004**, *59*, 2071−2088.
(10) Daniel, R. C.; Berg, J. C. Spreading on and Penetration into Thin, Permeable Print Media: Application to Ink-Jet Printing. *Adv. Colloid Interface Sci.* **2006**, *123−126*, 439−469.
(11) Clarke, A.; Blake, T. D.; Carruthers, K.; Woodward, A. Spreading and Imbibition of Liquid Droplets on Porous Surfaces. *Langmuir* **2002**, *18*, 2980−2984.
(12) Choi, M.; Son, G.; Shim, W. Numerical Simulation of Droplet Impact and Evaporation on a Porous Surface. *Int. Commun. Heat Mass Transfer* **2017**, *80*, 18−29.
(13) Starov, V. M.; Zhdanov, S. A.; Kosvintsev, S. R.; Sobolev, V. D.; Velarde, M. G. Spreading of Liquid Drops over Porous Substrates. *Adv. Colloid Interface Sci.* **2003**, *104*, 123−158.
(14) Hilpert, M.; Ben-David, A. Infiltration of Liquid Droplets into Porous Media: Effects of Dynamic Contact Angle and Contact Angle Hysteresis. *Int. J. Multiphase Flow* **2009**, *35*, 205−218.
(15) Denesuk, M.; Smith, G. L.; Zelinski, B. J. J.; Kreidl, N. J.; Uhlmann, D. R. Capillary Penetration of Liquid Droplets into Porous Materials. *J. Colloid Interface Sci.* **1993**, *158*, 114−120.
(16) Navaz, H. K.; Markicevic, B.; Zand, A. R.; Sikorski, Y.; Chan, E.; Sanders, M.; D'Onofrio, T. G. Sessile Droplet Spread into Porous Substrates-Determination of Capillary Pressure using a Continuum Approach. *J. Colloid Interface Sci.* **2008**, *325*, 440−446.
(17) Frank, X.; Perré, P. Droplet Spreading on a Porous Surface: A Lattice Boltzmann Study. *Phys. Fluids* **2012**, *24*, No. 042101.
(18) Oko, A.; Martinez, D. M.; Swerin, A. Infiltration and dimensional scaling of inkjet droplets on thick isotropic porous materials. *Microfluid. Nanofluid.* **2014**, *17*, 413−422.
(19) Tan, H. Absorption of picoliter droplets by thin porous substrates. *AIChE J.* **2017**, *63*, 1690−1703.
(20) Liu, Z.; Wang, Y.; Muzzio, F. J.; Callegari, G.; Drazer, G. Capillary Drop Penetration Method to Characterize the Liquid Wetting of Powders. *Langmuir* **2017**, *33*, 56−65.
(21) Barui, S.; Ding, H.; Wang, Z.; Zhao, H.; Marathe, S.; Mirihanage, W.; Basu, B.; Derby, B. Probing Ink−Powder Interactions during 3D Binder Jet Printing Using Time-Resolved X-ray Imaging. *ACS Appl. Mater. Interfaces* **2020**, *12*, 34254−34264.
(22) Starov, V. M.; Velarde, M. G.; Radke, C. J. *Wetting and Spreading Dynamics*; CRC Press: Boca Raton, FL, 2007; pp 354−368.
(23) Lucas, R. Veber das zeitgesetz *des kapillaren aufstiegs von flussigkeiten (Rate of Capillary Ascension of Liquids)*. *Kolloid-Z.* **1918**, *23*, 15−22.
(24) Washburn, E. W. The Dynamics of Capillary Flow. *Phys. Rev.* **1921**, *17*, 273−283.
(25) Chebbi, R. Dynamics of Liquid Penetration into Capillary Tubes. *J. Colloid Interface Sci.* **2007**, *315*, 255−260.
(26) Chebbi, R. Deformation of Advancing Gas−Liquid Interfaces in Capillary Tubes. *J. Colloid Interface Sci.* **2003**, *265*, 166−173.
(27) Beyer, W. H. *CRC Standard Mathematical Tables*, 27th ed.; CRC Press: Boca Raton, FL, 2000; p 128.